EUROPEAN SYNCHROTRON RADIATION FACILITY

INSTALLATION EUROPEENNE DE RAYONNEMENT SYNCHROTRON

ESRF

Experiment Report Form

ESRF	**Experiment title:** Pushing the limits of grating-based phase-contrast imaging for biomedical and paleontological applications	**Experiment number**: MI-983
Beamline: ID19	**Date of experiment**: from: 16/06-2010 to: 21/06-2010 10/11-2010 to: 15/11-2010	**Date of report**: January 31, 2011
Shifts: 2 x 15	**Local contact(s)**: Alexander Rack, Irene Zanette	*Received at ESRF:*

Names and affiliations of applicants **(* indicates experimentalists):**

- Prof. Dr. Franz Pfeiffer(*), Technichal University Munich, Germany
- Prof. Dr. Bert Mueller (*), University of Basel, Switzerland
- Dr. Timm Weitkamp (*), Synchrotron Soleil, Gyf-sur-Yvette, France
- Dr. Paul Tafforeau (*), ESRF Grenoble, France

1. Introduction & Motivation

The **overall goal** of this long-term proposal was (and still is) to establish a joined and coordinated effort to further push the current limitations of **grating-based phase-contrast imaging**, specifically for biomedical and paleontological applications.

As stated in the application proposal, the **main four technical development goals** of the whole experiment series in the three year duration of the LTP are:

(T1) **Increasing the density sensitivity** of grating-based phase-contrast tomography from currently ~ 1 mg/cm^3 to 0.2 mg/cm^3.

(T2) **Increasing the spatial resolution** of grating-based phase-contrast imaging from currently ~ 4 micron to below 1 micron.

(T3) **Increasing the energy range** of grating-based phase-contrast tomography from currently 25 keV to 90 keV.

(T4) **Development of a standardized and user-friendly** software package for grating-based phase-contrast tomography.

These technical goals are coupled to the following **scientific goals** :

(S1) The increased density sensitivity of < 0.2 mg/cm^3 will be used for establishing the potential of grating-based phase-contrast tomography for the **visualization of pathologies associated with neurodegenerative diseases.**

(S2) The increased special resolution of < 1 micron will be used for establishing the potential of grating-based phase-contrast tomography for the **visualization of brain micro-vessels in small-animal brains.**

(S3) The increased energy range of up to 90 keV will be used for establishing the potential of grating-based phase-contrast tomography in imaging of fossils, with specific aim on the **visualization of fossils such as inclusions in opaque amber and hominoid teeth at in the 1-40 microns resolution range.**

2. Experiments and Results so far

Within the long-term proposal we requested a total of six experiments each with 15 shifts distributed over 3 years. Up until now, three such experiment have been performed (November 2009, June 2010 and November 2010). We have already submitted a detailed experimental report for the experimental campaign in November 2009. This report now concerns beamtimes in 2010, in which the following scientific goals (as also outlined in the full proposal) could be achieved:

2.1. Characterization of detailed dependence of the soft-tissue sensitivity on experimental parameters, i.e., the inter-grating distance, grating period and x-ray energy (as described in work package T1.1 of the original proposal)

Several different geometries for the grating interferometer have been tested to characterize the density sensitivity and image quality of tomographic reconstructions of grating based phase-contrast imaging.
For high-resolution *and* high-sensitivity measurements of small samples (<3 mm) better results are obtained at low energies (<20 keV). Examples of this are given in the sections below.
For the investigation of small-animal tumour models, larger samples (~30 mm) must fit into the imaging field of view and higher x-ray energies are needed. As a part of our LTP we have optimized ex-vivo imaging of mice, by testing geometries corresponding to 35 keV (3rd and 5th fractional Talbot distance) versus 23 keV (5th fractional Talbot distance).

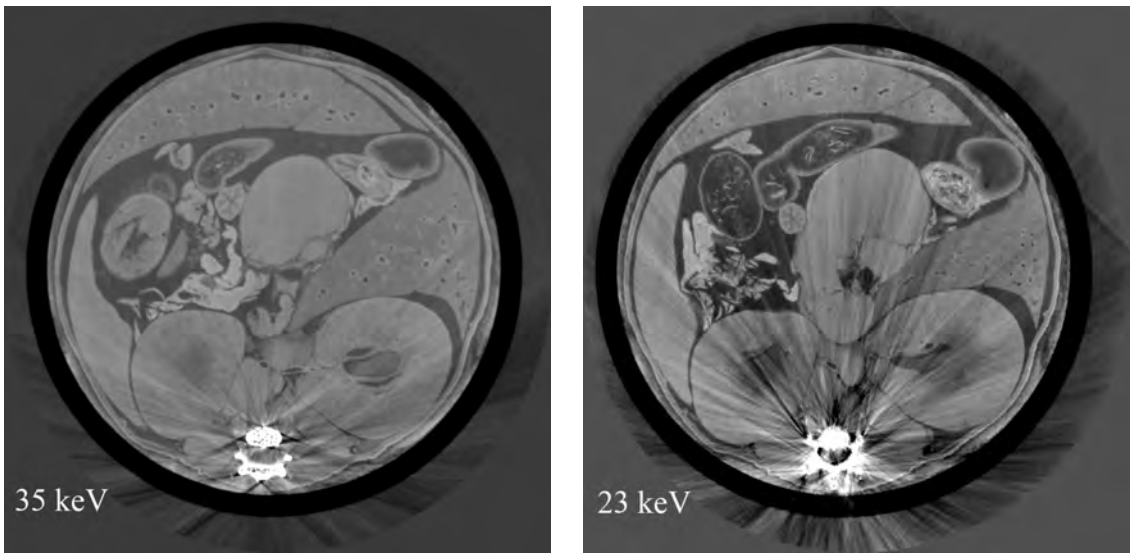

Figure 1: *Comparison of phase contrast tomograms of mouse fixated in formalin measured at 35 keV (left image) and at 23 keV (right image).*

The images displayed in Fig. 1 illustrate some of the effects and artifacts that influence the image quality of the reconstructed tomogram. At higher energy (35 keV), the sample shows less absorption and hence less artifacts from the highly absorbing bones (white features in the bottom of both images). At lower energy (23 keV) the density sensitivity is higher, giving better contrast to noise ratio in the soft tissue, but at the same time many streak-artefacts are observed from the bones.

As a conclusion, we can state that optimized image quality in this case is then a tradeoff between density resolution and reconstruction artifacts from hard tissue (bones). This is a so far non-observed effect in other phase-contrast imaging modalities.
In Fig. 1 both measurements were done with the sample submerged in a water container to suppress large phase effects from the sample edges. However, in cases where the sample is in a cylindrical tube (black ring on Fig. 1), equaly good results may be obtained without such a water container.

Figure 2: *Comparison of phase contrast tomograms of mouse fixated in formalin measured at 35 keV in a water container (left) and without a water container (right).*

As illustrated in Fig. 2, without compromizing the density resolution or image quality in general, the water container can be left out when the sample is in a cylindrical tube.
The result of these experiment are useful for future studies of small-animal tumour models in particular, and for planning more general user application of the grating interferometer at ID19, in general.

2.2. Increasing spatial resolution of grating-based phase-contrast imaging (work package T2.1 and T2.2 of the original proposal)

For our aim to improve the spatial resolution in phase grating interferometry down to less than 1 μm to visualize also the smallest vessels in tumors, we wanted to use small fractional Talbot distance (3^{rd} and 5^{th} FTD) at low energies.
Therefore components for a grating interferometer which should have been fixed to the high resolution sample stage at ID19 were developed and fabricated with the help of Jean-Paul Valade (ESRF, Grenoble, France). The requirements for the interferometer have been the high stability and the non-connectivity to the rotation stage to avoid movements during tomographic data acquisition. Parts of the mechanical setup, e.g., gratings, mounts, and motorized stages, which were used to construct the setup, were kindly supported by Christian David (PSI, Villigen, Switzerland) and Franz Pfeiffer (Technical University Munich). The absorption grating was used with a pitch of 2 μm. Therefore the spatial resolution was not expected to be better than 2 μm in this experiment. The phase grating exhibit a pitch of 4 μm and a phase shift of π. The detector pixel size was chosen to be 1.5 μm giving a field of view of less than 3 mm.

Table 1, Figure 3, and Figure 4 show results of experiments, in which the spatial resolution of grating-based phase-contrast imaging was experimentally assessed using **well defined resolution test objects**, such as wedge-shaped samples (edges SiNi windows) and Siemens-start resolution test objects.

Object	Resolution [µm] ER:±1.5 µm	Detector Pixel Size [µm]	Phase Grating	Absorption Grating	Talbot Distance	Eyepiece
nitride membrane	5,6114	1,875	ID19a	10G	2	2
nitride membrane	4,6027	1,875	ID19a	10C	3	2
nitride membrane g1b	4,2223	1,875	ID19a	10C	3	2
nitride membrane	4,8914	1,875	ID19a	10G	3	2
nitride membrane	3,8633	1,5	ID19a	10G	5	1
nitride membrane	4,3602	1,875	ID19a	10G	5	2
siem1mm	4,9500	1,5	ID19a	10G	5	1
siem1mm	4,7521	1,5			5	1
siem2mm	3,7155	1,5	ID19a	10G	5	1
siem2mm	3,3943	1,875	ID19a	10G	2	2
siem2mm	3,6913	1,875	ID19a	10G	3	2
siem2mm	5,0437	1,875	ID19a	10G	5	2
siem2mm	5,8379	1.875	ID19a	10G	5	2

Table 1: *The Table shows the determined spatial resolution using the Siemens Star and the Edge Response function of a measured nitride membrane. The settings vary in the detector pixel size which was dependent on the eye piece selection.*

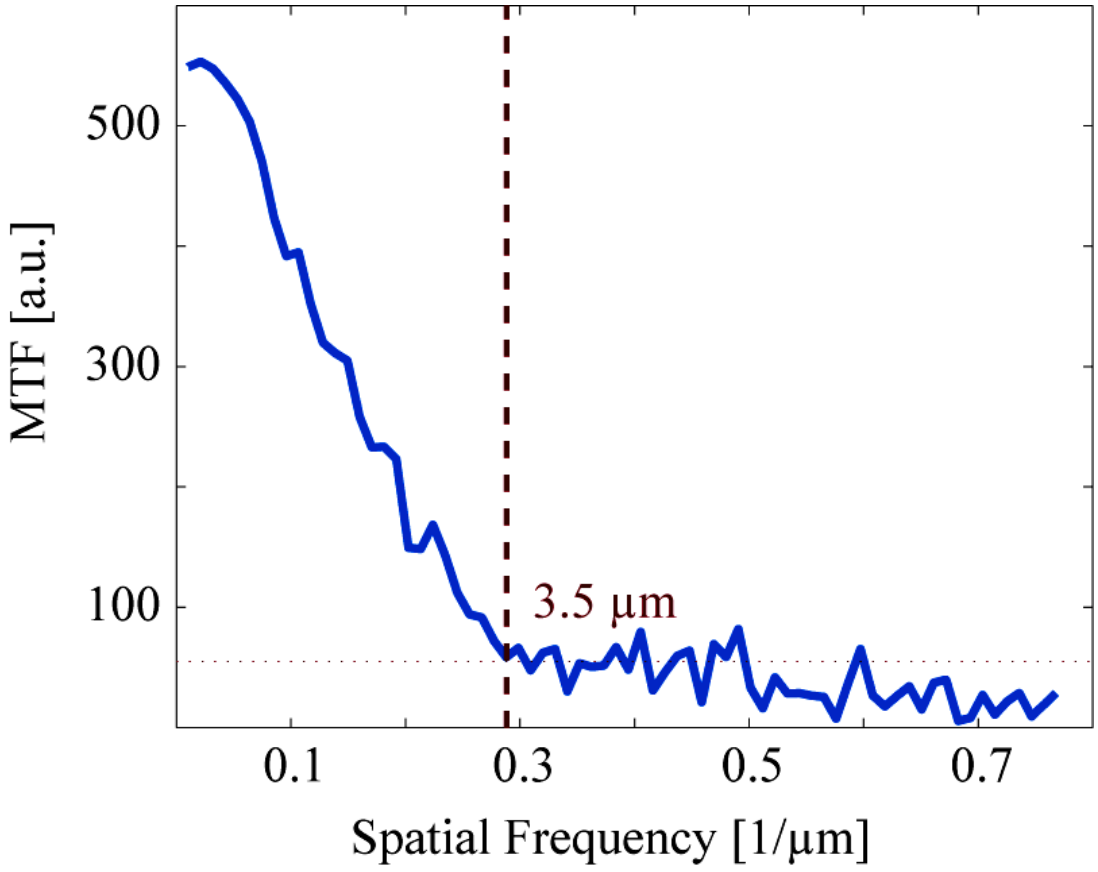

Figure 3: *Using a nitride membrane the contrast is sufficient enough to determine the edge response function (ERF) which can be used to calculate the modulation transfer function (MTF). The Spatial Frequency at 10% MTF provides the spatial resolution.*

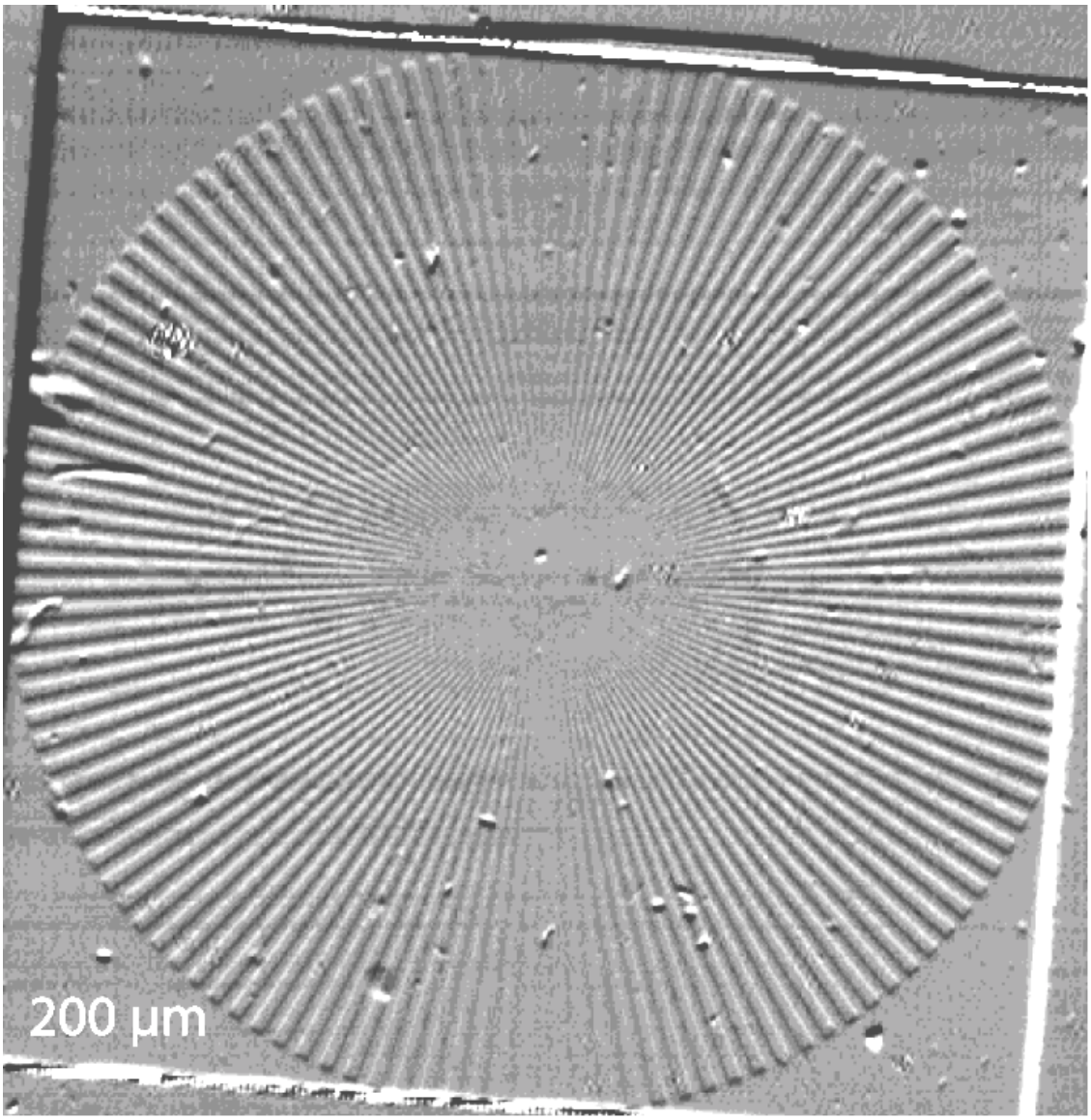

Figure 4: *The projection of the Siemens Star can be used to determine the spatial resolution by calculating the diameter where the fins can not be distinguished anymore. The Siemens Stars were kindly supported by C. David (PSI, Villigen, Switzerland).*

Concerning **high-resolution measurements of biological samples**, several tumors have been examined (see Figure 5 and Table 2). They were grown at the institute of biomedical engineering in Zurich. For this C51 tumor cells were injected in six nude mice and observed due to their growth. When the diameter of the tumor reached shortly below 3 mm it was extracted and fixed in para-formaldehyde (PFA) 5%.

Using small Talbot distances will improve the spatial resolution but reduce the contrast resolution in the tomographic data. Therefore the measurements were carried out at 17.6 keV.
Because high photon statistics are required for the high resolution detectors the phase gratings were thinned down to 300 µm. Additionally we had abstained from the use of a water tank in which the sample or sample container is measured. The absence of the water tank caused phase wrapping between the sample/container and the air. Therefore a "no-tank correction" was needed before phase retrieval calculations. An algorithm for that task was written by Timm Weitkamp (Synchrotron Soleil, Gif-Sur-Yvette, France).

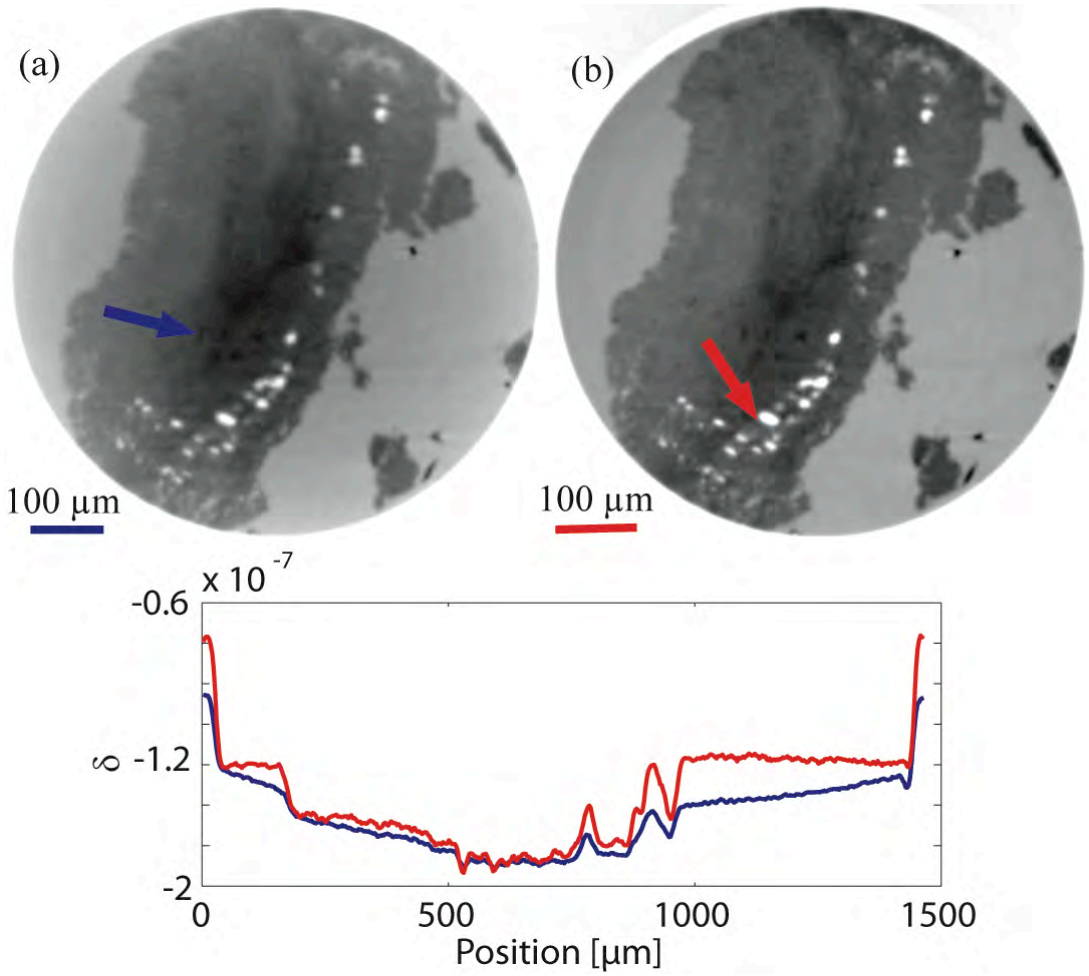

Figure 5: *Phase contrast tomograms of tumor tissue with (a) and without (b) the "no-tank correction". The plot shows clearly that the "no-tank correction" could reduce the cupping effect in (a). In both images one can see some blood vessels (arrow in (a)) and fat cells (arrow in (b)). The increasing vessel density in the center of the specimen let presume that strong neo vascularization took place.*

Scan No	Name	Sample	#Projections	Size	Exposure time [ms]	Pixel Size [µm]
1	tumor_2_TD5_1a	C51 tumor in PFA 5%	1580	2048x360	0,4	1.875
2	tumor_3_TD5_1a	C51 tumor in PFA 5%	1580	2048x360	0,4	1.875
	tumor_3_TD5_1b	C51 tumor in PFA 5%	1580	2048x360	0,4	1.875
	tumor_3_TD5_1c	C51 tumor in PFA 5%	1580	2048x360	0,4	1.875
	tumor_3_TD5_1d	C51 tumor in PFA 5%	1580	2048x360	0,4	1.875
3	tumor_4_TD5_1a	C51 tumor in PFA 5%	360	2048x1580	0,4	1.875
	tumor_4_TD5_1b	C51 tumor in PFA 5%	360	2048x1580	0,4	1.875
	tumor_4_TD5_1c	C51 tumor in PFA 5%	360	2048x1580	0,4	1.875
	tumor_4_TD5_1d	C51 tumor in PFA 5%	360	2048x1580	0,4	1.875
4	tumor_5_TD5_2a	C51 tumor in PFA 5%	360	1024x788	0,3	3
	tumor_5_TD5_2b	C51 tumor in PFA 5%	360	1024x788	0,3	3
5	tumor_6_TD5_2a	C51 tumor in PFA 5%	360	1024x788	0,3	3
	tumor_6_TD5_2b	C51 tumor in PFA 5%	360	1024x788	0,3	3
6	tumor_6_TD5_3	C51 tumor in PFA 5%	800	2048x1576	0,3	1.5

Table 2: *The table above listed the successfully measured tumor samples at ID19 using differential phase contrast µCT. The itemization (abc) describes the measurement of the same sample at the same height step but with shifted rotation angle. All samples were measured at the 5th fractional Talbot distance.*

Tips of pipettes were used as containers for the tumor samples because they reveal thin walls and cylindrical shape which is important for the "no-tank correction". Additionally pipette tips with diameter below 3 mm are available. The material of the pipettes were supposed to be similar to Polymethylmethacrylat which had shown less phase contrast deviation in comparison to soft tissue in previous experiments.

Five tumor samples were measured at the 5th fractional Talbot distance (14 mm) at exposure times in the range of [0.2-0.4] ms (see table 1).
One big problem that occurred during the experiments was the strong bubble development. Therefore different efforts to reduce this problem were carried out. Before every scan the tumor samples were degassed in a vacuum chamber at approximately 5 mbar. Previous experiments have shown a reduction in the bubble development when removing the gas from the sample and from the formalin.
The bubble development did not appear instantly after imaging has started. Therefore we carried out two identical measurements of one sample with reduced number of projection to reduce the scan time and therefore the possibility for the bubble development. The rotation angles between the two data sets are shifted to each other. In case no bubbles occurred during the full measurements the data set can be reassembled again giving high quality data. In case the bubble development occurred only in one data set at least one data set is available.
It was presumed nevertheless that the bubble development is flux dependent and not only time dependent therefore the wiggler gap was increased to reduce flux on sample. Additionally the pixel size was increased up to 1.875 μm by changing the eyepiece or 3 μm by pixel binning.

Immediately after LTP MI983 measurement of the tumor tissue in June 2010, holotomography measurements were carried out during MD 498 where tumor samples were measured under the same condition as it was for the differential phase contrast experiment. A publication about these results is in preparation.

2.3. Development of standardized and user-friendly software package for grating-based phase-contrast tomography (work package T4.1 of the original proposal)

Online data analysis code was developed by the ESRF partners (Zanette, Weitkamp) for automated pre-processing of the raw data. This code is written in IDL and runs on the NICE computer cluster. The pre-processing includes the following steps:

- Automatic recognition of scan parameters;
- Dark-image correction;
- Processing of phase-stepping scans and extraction of differential phase images, pseudo-absorption images, and dark-field images;
- Flat-field correction of the processed images;
- De-trending of the processed differential phase images;
- Output of processed, corrected projection images to disk;
- (optional) Output of sinograms to disk.

The output data can be used as input for the tomographic reconstruction program system PyHST, developed at the ESRF.

To this end, PyHST has been extended by A. Mirone for phase tomographic reconstruction from differential phase projections: the imaginary sign filter and an appropriate scaling factor have been included in the reconstruction program.

Complete documentation for users on how to use the pre-processing algorithm and the PyHST program for grating-based tomography is now available on the ID19 wiki page.

2.4. Grating-based phase-contrast tomography with high spatial resolution (work package S1.1 and S2.1 of the original proposal)

In connection with this LTP a series of studies aiming at high spatial resolution and high density sensitivity has been carried out. Figures 6 and 7 illustrate a successful experiment of a human cerebellum fixated in formalin, carried out at an x-ray energy of 23 keV with the grating interferometer in the 9th fractional Talbot distance. The effective pixel size of the FReLoN CCD was 5.1 μm with 2048x2048 pixels corresponding to

10.2 mm^2 field-of-view. Figure 6 allows a clear differentiation between the morphological features of the human cerebellum like gray (a,c) and white (b) matter.

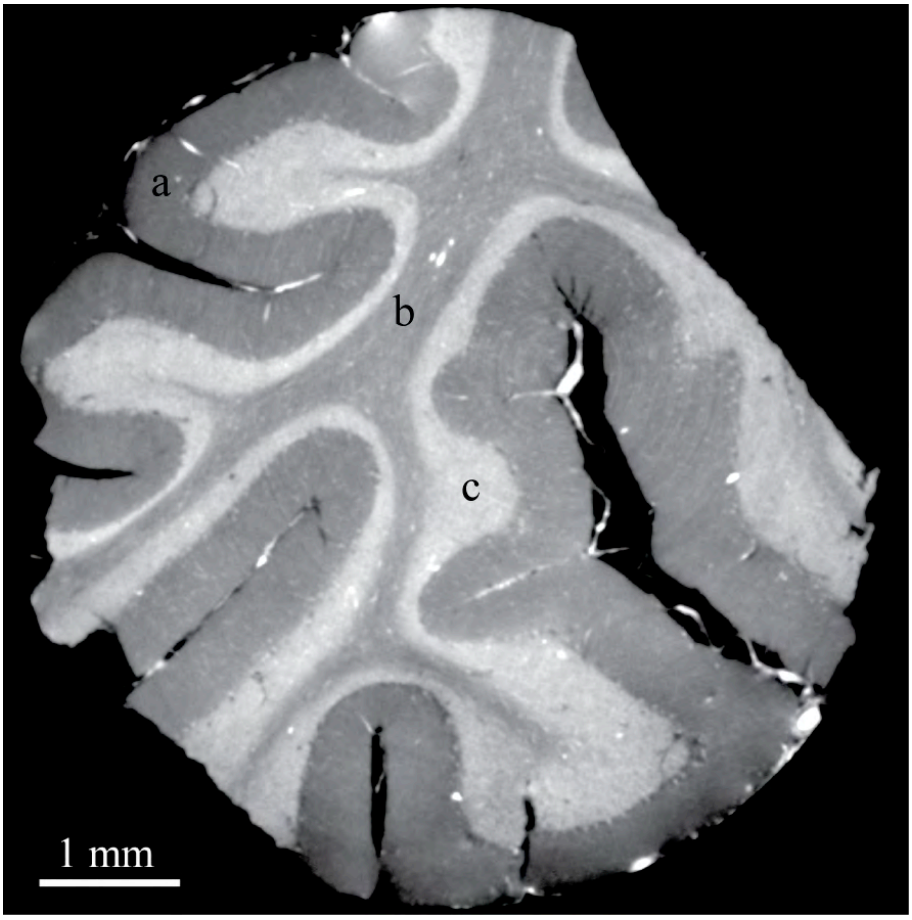

Figure 6: *One reconstructed phase contrast slice showing the successful differentiation between the stratum moleculare (a) and the stratum granulosum (b), which both belong to gray matter, and the white matter (b).*

Figure 7 even demonstrates the three-dimensional visualization of individual Purkinje cells without the aim of any contrast agents. The segmentation of the cells resulted by simple intensity-base segmentaion.

The results have been published in *Journal of the Royal Society, Interface*, vol. 7, Dec. 2010, pp. 1665-76 and in the ESRF Spotlight on science (5-11-2011) and Scientific Highlights 2010, pp 108-9.

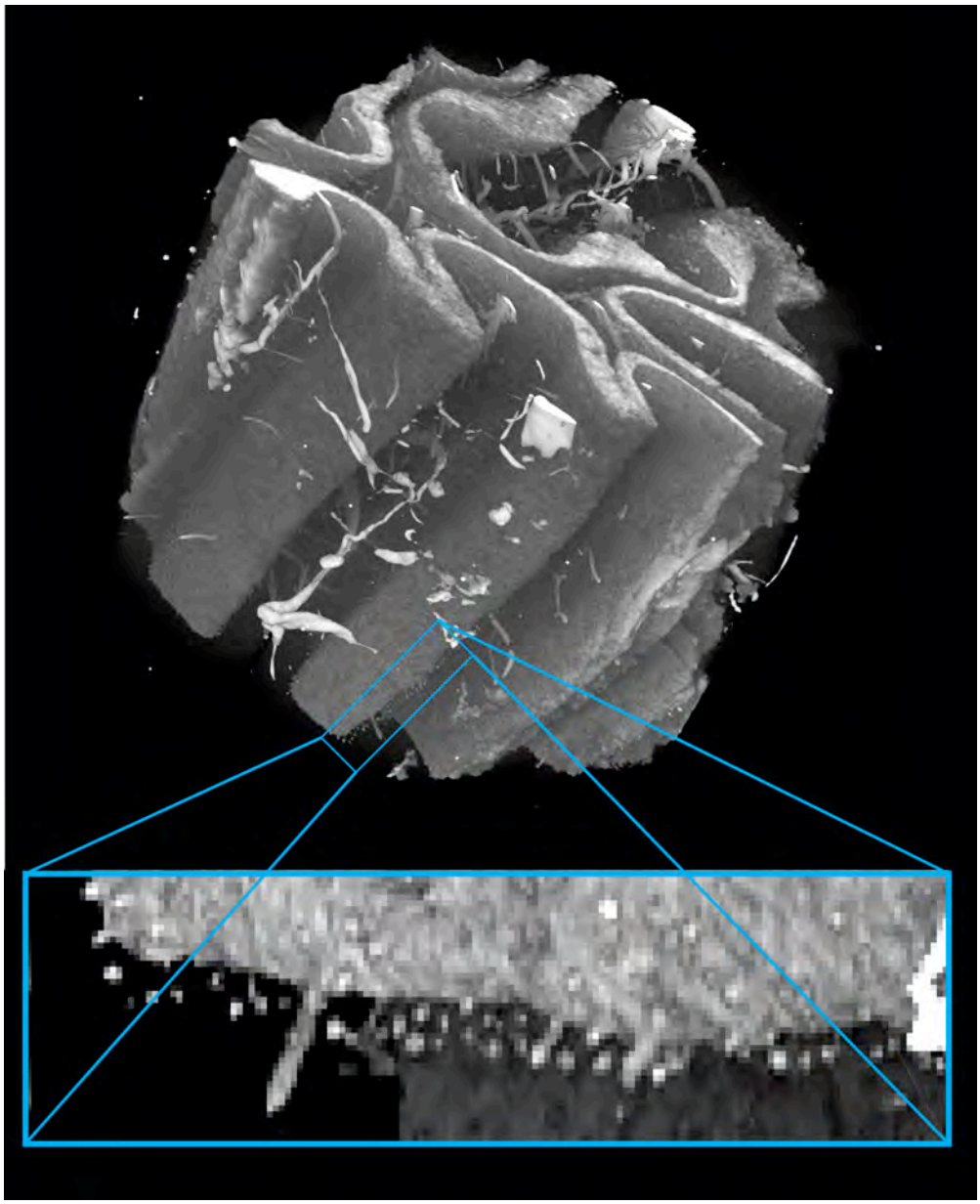

Figure 7: *Phase-contrast three-dimensional rendering of an human cerebellum block. The intensity-based segmentation of the stratum granulosum and the blood vessels allows the three-dimensional visualization of the so-called Purkinje cells (the diameter of each cell is ~40 µm) along the surface of stratum granulosum.*

2.3. Demonstration of phase-contrast tomography of paleontological test samples at 82 keV (work package T3.2 and S3.2 of the original proposal)

For paleontology studies, very high x-ray energies are necessary to penetrate samples such as fossilized teeth (from orang-utan), as the transmission is too low at lower x-ray energies.

Figure 8 displays the results of a proof-of-principle tomography experiment carried out in the framework of this LTP, on a fossilized tooth provided by Paul Tafforeau/ ESRF.

While several improvements can still be made, this result demonstrates a first proof-of-priniciple experiment of high energy phase-contrast CT beyond 80 keV.

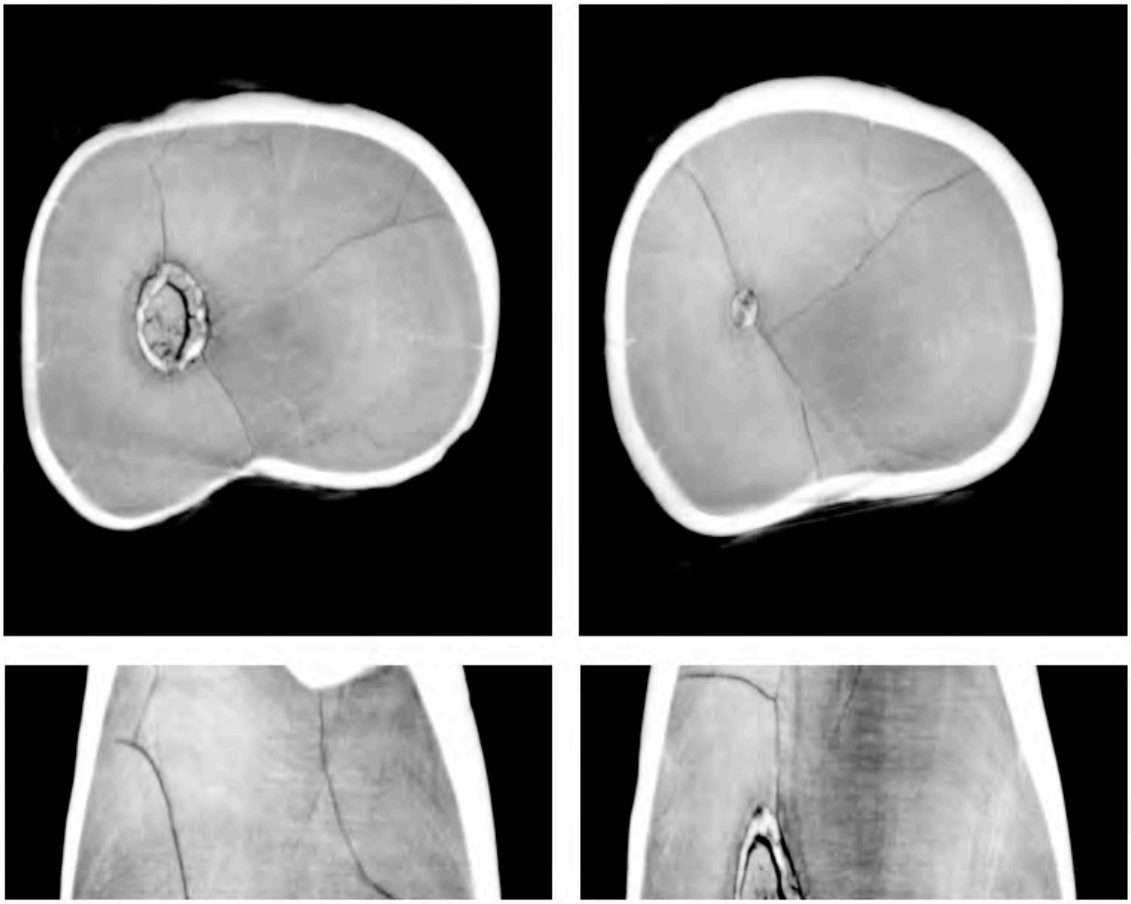

Figure 8: *Grating-based phase-contrast micro-tomography results for a fossilized human tooth at 82 keV x-ray energy. Two axial (top) and two frontal (bottom) slices through the reconstructed phase contrast volume are shown. It is worth noting that particualry the frontal slices show clearly the dental development rings, whose micro-morphology presents important information to the paleontologist.*

Finally, the dark-field signal obtained from the grating interferometer has been explored to image the scattering caused by sub-micron structures in the sample, and to map the orientation of fibrestructures. In connection with the experiment done in this LTP, we have studied the orientation of dentin, enamel and pulp structure in a human tooth slice (see Figure 9).

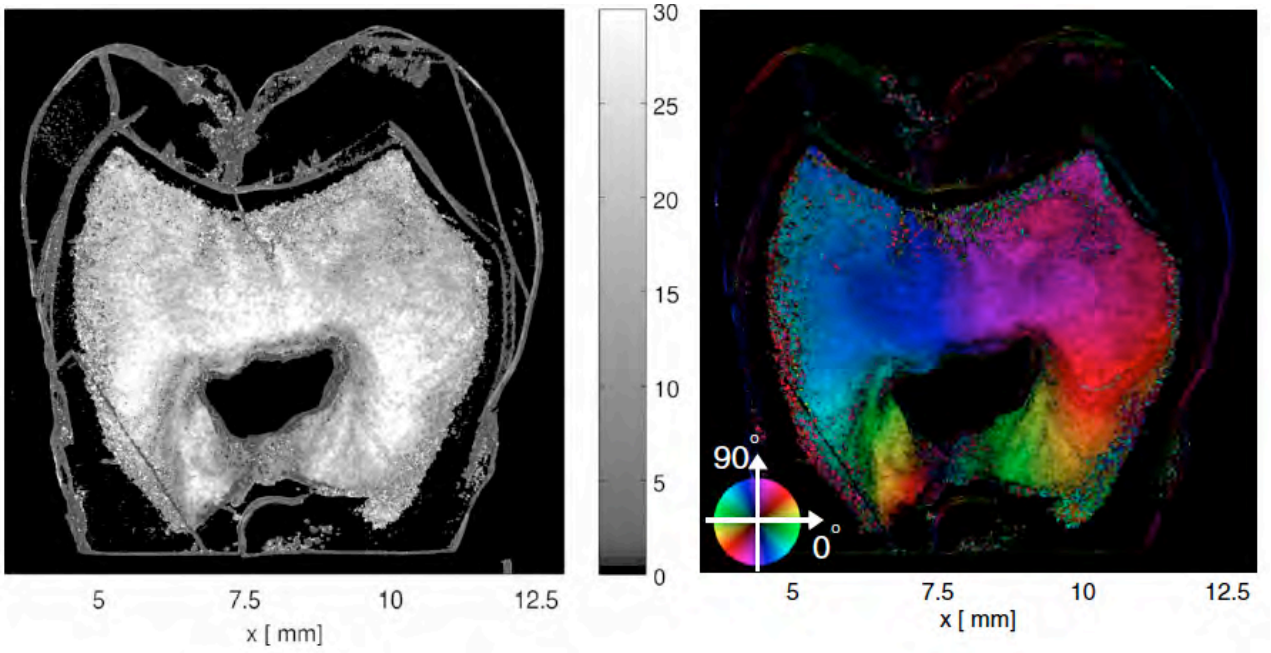

Figure 9: *Grating-based directional dark-field results for a human. Left panel: Scattering eccentricity is displayed such that fribrous structures appear bright, and areas of homogeneous scattering appear dark. Right panel: Directional dark-field, displaying the orientation of the fibrous structures in the tooth pulp.*

3. Dissimination of the results

Parts of the results from these experiments have been presented at conferences and in the corresponding proceedings. More publications are in preparation and will be submitted in 2011. The published or accepted articles related to this work are listed here:

Publications:

[1] M. Bech, T.H. Jensen, O. Bunk, T. Donath, C. David, T. Weitkamp, G. Le Duc, A. Bravin, P. Cloetens, and F. Pfeiffer, "Advanced contrast modalities for X-ray radiology: Phase-contrast and dark-field imaging using a grating interferometer" *Zeitschrift fur medizinische Physik*, vol. 20, Mar. 2010, pp. 7-16.

[2] F. Pfeiffer, C. David, O. Bunk, C. Poitry-Yamate, R. Grütter, B. Müller, and T. Weitkamp, "High-sensitivity phase-contrast tomography of rat brain in phosphate buffered saline," *Journal of Physics: Conference Series*, vol. 186, Sep. 2009, p. 012046.

[3] G. Schulz, T. Weitkamp, I. Zanette, F. Pfeiffer, F. Beckmann, C. David, S. Rutishauser, E. Reznikova, and B. Müller, "High-resolution tomographic imaging of a human cerebellum: comparison of absorption and grating-based phase contrast" *Journal of the Royal Society, Interface / the Royal Society*, vol. 7, Dec. 2010, pp. 1665-76.

[4] T. Jensen, M. Bech, I. Zanette, T. Weitkamp, C. David, H. Deyhle, S. Rutishauser, E. Reznikova, J. Mohr, R. Feidenhans'l, and F. Pfeiffer, "Directional x-ray dark-field imaging of strongly ordered systems," *Physical Review B*, vol. 82, Dec. 2010.

[5] T. Weitkamp, I. Zanette, C. David, J. Baruchel, M. Bech, P. Bernard, H. Deyhle, T. Donath, J. Kenntner, S. Lang, J. Mohr, B. Müller, F. Pfeiffer, E. Reznikova, S. Rutishauser, G. Schulz, A. Tapfer, and J.-P. Valade, "Recent developments in x-ray Talbot interferometry at ESRF-ID19," *Proceedings of SPIE*, vol. 7804, 2010, pp. 780406-780406-10.

[6] G. Schulz, A. Morel, M.S. Imholz, H. Deyhle, T. Weitkamp, I. Zanette, F. Pfeiffer, C. David, M. Müller-Gerbl, and B. Müller, "Evaluating the microstructure of human brain tissues using synchrotron radiation-based micro-computed tomography," *Proceedings of SPIE*, vol. 7804, 2010, p. 78040F-78040F-8.

[7] T.H. Jensen, A. Böttiger, M. Bech, I. Zanette, T. Weitkamp, S. Rutishauser, C. David, E. Reznikova, J. Mohr, L.B. Christensen, E.V. Olsen, R. Feidenhans'l, and F. Pfeiffer, "X-ray phase-contrast tomography of porcine fat and rind", *Meat science*, accepted 2010.

[8] I. Zanette,M. Bech, F. Pfeiffer, and T. Weitkamp, "Interlaced Phase Stepping in Phase-Contrast X-Ray Tomography", *Applied Physics Letters*, Accepted 2011.